ADVANCED FUNCTIONAL MATERIALS
www.afm-journal.de

Boosting H_2O_2-Guided Chemodynamic Therapy of Cancer by Enhancing Reaction Kinetics through Versatile Biomimetic Fenton Nanocatalysts and the Second Near-Infrared Light Irradiation

Tingting Wang, Hao Zhang, Hanghang Liu, Qiang Yuan, Feng Ren, Yaobao Han, Qiao Sun, Zhen Li, and Mingyuan Gao*

Fenton reaction–based chemodynamic therapy (CDT) has attracted considerable attention for tumor treatment, because the Fenton reaction can degrade endogenous H_2O_2 within the tumor to form reactive oxygen species (ROS) to kill cancer cells. The kinetics of the Fenton reaction has significantly influenced its treatment efficacy. It is crucial to enhance the reaction kinetics at the maximum H_2O_2 concentration to quickly produce vast amounts of ROS to achieve treatment efficacy, which to date, has not been realized. Herein, reported is an efficacious CDT treatment of breast cancer using biomimetic CS-GOD@CM nanocatalysts, which are rationally designed to significantly boost the Fenton reaction through improvement of H_2O_2 concentration within tumors, and application of the second near-infrared (NIR-II) light irradiation at the maximum concentration, which is monitored by photoacoustic imaging. The biomimetic nanocatalysts are composed of ultra-small $Cu_{2-x}Se$ (CS) nanoparticles, glucose oxidase (GOD), and tumor cell membrane (CM). The nanocatalysts can be retained in tumor for more than two days to oxidize glucose and produce an approximately 2.6-fold increase in H_2O_2 to enhance the Fenton reaction under the NIR-II irradiation. This work demonstrates for the first time the CDT treatment of cancer enhanced by the NIR-II light.

1. Introduction

Fenton reaction–based chemodynamic therapy (CDT) as an emerging nanocatalytic treatment has attracted increasing interest in recent years, because it uses endogenous chemicals (e.g., H_2O_2) overproduced in cancer cells to generate reactive oxygen species (ROS) to kill cancer cells.[1–3] The overproduced H_2O_2 in cancer cells is efficiently degraded under the catalysis of versatile metal ions (e.g., Fe^{2+}, Mn^{2+}, Cu^{+}, Pt^{2+}, Co^{2+}, and V^{2+}) to produce hydroxyl (•OH) radicals for treatment.[4–8] Thereby, the generation of •OH radicals plays a significant role and determines the efficacy of CDT treatment.[9] Although advances in nanotechnology offer a promising way to facilitate cancer therapy through Fenton reaction,[10] there are some challenges that remain to be solved for improving the efficacy of treatment. One of them is the reaction kinetics of Fenton reaction, and how to maximally speed up the Fenton reaction in a controllable way has been a challenge for enhancing the efficacy of therapy.

The reaction kinetics of Fenton reaction strongly depends on the performance of catalysts and reaction parameters. For example, Fe^{2+} ions and their based materials could be an excellent Fenton catalyst in a low pH range from 2.0 to 4.5, but the high pH in cancer (pH = 6.5–6.9) significantly degrades the performance of Fe^{2+} ions in the Fenton reaction for cancer therapy.[1,4] To enhance their performance, the UV light was used to reduce Fe^{3+} ions into Fe^{2+} ions for recycling of Fenton reaction.[11–15] Since the UV light has limited penetration depth, up-conversion nanoparticles have been used to convert near-infrared (NIR) light into UV light for photo-Fenton reaction to improve its therapeutic efficacy.[16] However, the conversion efficiency could drastically influence the kinetics of Fenton reaction. Another option is the deposition of Fenton catalysts on the surface of nanomaterials with NIR absorbance to enhance Fenton reaction. For example, He et al. deposited iron hydroxide/oxide particles on the surface of graphene oxide sheets to boost the generation of ROS under the NIR irradiation.[17] For these hybrid Fenton catalysts, their performance is strongly dependent on the electron and energy transfer between their interface under the NIR irradiation. Therefore, great efforts have been devoted to rationally design

T. Wang, Dr. H. Zhang, H. Liu, F. Ren, Y. Han, Prof. Q. Sun, Prof. Z. Li, Prof. M. Gao
Center for Molecular Imaging and Nuclear Medicine
State Key Laboratory of Radiation Medicine and Protection
School for Radiological and Interdisciplinary Sciences (RAD-X)
Soochow University
Collaborative Innovation Center of Radiation Medicine of Jiangsu Higher Education Institutions
Suzhou 215123, P. R. China
E-mail: zhenli@suda.edu.cn
Q. Yuan
The Second Affiliated Hospital of Soochow University
Suzhou 215004, P. R. China
The ORCID identification number(s) for the author(s) of this article can be found under https://doi.org/10.1002/adfm.201906128.

DOI: 10.1002/adfm.201906128

and develop different kinds of high-performance Fenton catalysts by engineering their size, shape, composition, and crystal structure. Several types of Fenton-like catalysts based on Mn^{2+}, Cu^{+}, Pt^{2+}, Co^{2+}, and V^{2+} ions were developed, of which Cu^{+}-based Fenton catalysts could be a better candidate, due to their broader reaction pH range in comparison with Fe^{2+}-based catalysts.[4]

Among different Cu^{+}-based Fenton catalysts, ultra-small $Cu_{2-x}Se$ nanoparticles are expected to show excellent performance in CDT treatment of cancer because of their unique properties, which has not been fully investigated. Their abundant Cu^{+} ions could catalyze the Fenton reaction in a wider range of pH. More importantly, ultra-small $Cu_{2-x}Se$ nanoparticles exhibit a strong NIR localized surface plasmon resonance (LSPR) in the range of 600–1100 nm. They not only can efficiently absorb both NIR-I and NIR-II light, where I and II refer to the first (700–900 nm) and the second (1000–1700 nm) NIR windows, and convert it into heat to speed up the Fenton reaction, but also can enhance the Fenton reaction via electron and energy transfer under NIR-II irradiation.[18,19]

Compared with UV and visible light, NIR-II light has deeper penetration for tumor therapy. Therefore, nanoparticles with strong NIR-II absorbance have attracted considerable interest for the NIR-II photoacoustic (PA) imaging and photothermal therapy (PTT). There are several types of such nanomaterials, including inorganic nanostructures (e.g., single-wall carbon nanotubes,[20] quantum dots,[21] and rare-earth-doped nanoparticles),[22] small organic molecule-based nanoparticles (e.g., BBTD-based molecules),[23] and semiconducting polymer nanoparticles (SPNs),[24] of which SPNs have been extensively studied for NIR-II PA imaging and PTT.[25–27] However, there is no report on the photo-Fenton reaction directly enhanced by the NIR-II light.

Besides the performance of Fenton catalysts, the reaction kinetics of Fenton reaction is also strongly relied on the reaction parameters, such as the concentration of H_2O_2 within tumor, which is still not high enough for producing large amounts of $^{\bullet}OH$ radicals to kill cancer cells. It is extremely important to elevate the contents of H_2O_2 in the tumor to speed up the Fenton reaction for the treatment of cancer. To solve this issue, wrapping of exogenous H_2O_2 was proposed.[28] It is difficult, however, to completely deliver the wrapped H_2O_2 to the tumor site, and H_2O_2 could leak from the wrapping materials and cause damage to normal tissues during delivery.[29] An alternative option is the in situ generation of H_2O_2 within the tumor. Since glucose (Glu) in tumor cells is more abundant than in normal cells due to the Warburg effect,[30] glucose oxidase (GOD) as a natural aerobic dehydrogenase has been used to catalyze the oxidation of glucose in tumors to generate H_2O_2 for enhancing the Fenton reaction in situ.[31,32] This in situ production is relatively safer than delivery of exogenous H_2O_2.[33]

In addition to oxidizing the Glu in the tumor, however, GOD could also oxidize Glu in normal cells and induce damage to normal tissues. There are several ways to reduce the side effects of GOD on normal tissues. One popular way is to use the tumor microenvironment to control the release of GOD. For example, Li et al. encapsulated GOD with copolymers, in which the GOD remained inactive in normal tissues under neutral conditions and could be released under the weak acidic conditions in the tumor.[34] Zhang et al. also encapsulated GOD with degradable MnO_2,[35] which can be decomposed in the tumor acidic microenvironment to release GOD. Furthermore, in order to improve the biocompatibility and targeting ability of nanoparticles, cell membranes (CMs) were also used to coat the GOD and reduce its exposure to avoid toxicity and improve homologous adhesion.[36]

In addition to the H_2O_2 content, the reaction kinetics of Fenton reaction could be further enhanced by increasing the temperature of tumor site. For example, Liu et al. developed an "all-in-one" Fe_2P Fenton agent, which showed an excellent photothermal effect toward speeding up the Fenton reaction under NIR irradiation.[37]

The above description clearly demonstrates that the reaction kinetics of Fenton reaction for tumor therapy could be increased by engineering high-performance Fenton catalysts, and tuning reaction parameters such as the concentration of H_2O_2 and reaction temperature at tumor site. However, the time-dependent variation of H_2O_2 in tumor was not known and monitored, which leads to the difficulty in determining the optimal time for applying external stimulation to enhance the Fenton reaction. In addition, there is lack of effective external stimulation to drastically enhance the Fenton reaction. Therefore, it is crucial to simultaneously apply different internal and external strategies to maximally enhance the Fenton reaction for achieving excellent efficacy of CDT treatment, which has not been well realized.

In this work, we significantly enhanced the kinetics of Fenton reaction for CDT treatment of breast cancer by using rationally designed biomimetic CS-GOD@CM nanocatalysts in conjunction with the NIR-II irradiation (**Scheme 1**). The NIR-II irradiation was applied when the maximum concentration of H_2O_2 within tumor was achieved, which was monitored by highly sensitive PA imaging. To our best knowledge, there is no report on the NIR-II photo-enhanced Fenton reaction for tumor therapy. We conjugated GOD with ultrasmall $Cu_{2-x}Se$ nanoparticles (with the composite designated as CS-GOD nanoparticles) to increase the content of H_2O_2 through in situ oxidization of the Glu within tumor by GOD. The CS-GOD conjugates were coated with 4T1 CMs (with the composite designated as CS-GOD@CM nanoparticles) to avoid the exposure of GOD to normal tissue and improve the homologous adhesion of nanoparticles to the solid tumor after tail vein injection. The CS-GOD@CM nanoparticles could be efficiently accumulated in the solid tumor for more than 48 h, and their accumulation was three times greater than for the nanoparticles without CM encapsulation. The accumulation of nanoparticles and the variations of H_2O_2 and O_2 in tumor can be characterized by PA imaging. Due to the efficient accumulation of CS-GOD@CM nanoparticles, the H_2O_2 concentration was significantly increased and reached its maximum 36 h post-injection, when NIR irradiation from a 1064 nm laser was applied to speed up the Fenton reaction to rapidly generate vast amounts of ROS radicals. The results demonstrate that the Fenton reaction had been drastically boosted to successfully eliminate 4T1 solid tumors under NIR-II light irradiation.

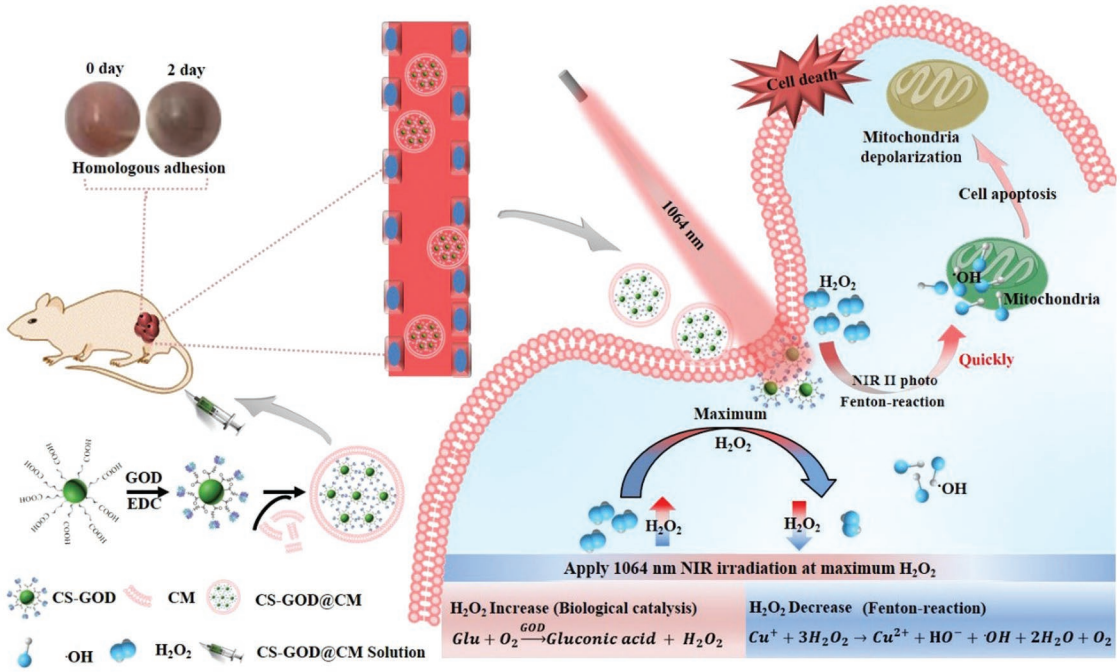

Scheme 1. Schematic illustration of the Fenton reaction enhanced by NIR-II window irradiation guided by H_2O_2 concentration in tumor for the treatment of breast cancer.

2. Results and Discussion

2.1. Design and Characterization of CS-GOD@CM Nanoparticles

The uniform water-soluble $Cu_{2-x}Se$ nanoparticles (designated as CS) were synthesized by a mild approach as described elsewhere.[38,39] In order to carry GOD for the oxidation of glucose, CS nanoparticles were functionalized with bifunctional COOH-PEG-SH, where functional carboxylic groups (-COOH) were then conjugated with GOD under catalysis by 1-ethyl-3-(3-dimethylaminopropyl)carbodiimide hydrochloride (EDC). The resultant conjugates were designated as CS-GOD nanoparticles.[40] To reduce the exposure of GOD and improve the homologous adhesion of CS-GOD nanoparticles, 4T1 CMs were coated onto them (**Figure 1**a), and the obtained nanoparticles were denoted as CS-GOD@CM nanoparticles. Both CS-GOD nanoparticles and CS-GOD@CM nanoparticles were characterized by transmission electron microscope (TEM) to be (4.8 ± 0.5) and (39 ± 2.0) nm, respectively (Figure 1b and Figure S1a,b, Supporting Information).[41] Their particle sizes are rather consistent with those obtained from dynamic light scattering (DLS) measurements (Figure S1c, Supporting Information).[42] The zeta potentials of CS nanoparticles, CS-GOD nanoparticles, and CS-GOD@CM nanoparticles displayed in Figure S1d in the Supporting Information indicate the successful conjugation of CS nanoparticles with GOD, as well as the coating of the resultant nanoparticles with cancer CMs. Furthermore, the sulfate-polyacrylamide gel electrophoresis (SDS-PAGE) was used to analyze the CM proteins (Figure 1c). The results show that both the cancer CM vesicles and CS-GOD@CM nanoparticles possess the similar proteins compared with those of 4T1 CM, which demonstrates the successful coating of CM onto CS nanoparticles.

Due to the homologous adhesion effect, the successful encapsulation of CS-GOD nanoparticles with 4T1 CM can significantly enhance cellular uptake by 4T1 cells, which was confirmed by the results of confocal laser scanning microscopy (CLSM) shown in Figure 1d. To demonstrate the homologous adhesion effect, three types of cells (3T3, U87, and 4T1 cells) were, respectively, cultured with 3,3′-dioctadecyloxacarbocyanine perchlorate (DiO)-labeled CS-GOD@CM nanoparticles (12.5 μg mL^{-1}) for 1 h. The stronger green fluorescence (FL) observed in 4T1 cells than those of 3T3 and U87 cells suggests that CS-GOD@CM nanoparticles were efficiently taken up by 4T1 cells. These results demonstrate that CS-GOD@CM nanoparticles can be highly and specifically recognized by the same cell lines in vitro, and suggest excellent self-targeting ability to the homologous tumors in vivo.[43] This homologous adhesion effect ensures that CS-GOD@CM nanoparticles have good capability of targeting 4T1 solid tumors so as to reduce their harm to normal tissues.

As described in Equation (1), GOD can catalyze the oxidation of glucose (Glu) into gluconic acid and H_2O_2, which leads to a decrease in the pH of the reaction solution and an increase in the H_2O_2 concentration. The thus-formed H_2O_2 can be immediately degraded by CS nanoparticles to release O_2 as described in Equation (2)

$$Glu + O_2 \xrightarrow{GOD} Gluconic\ acid + H_2O_2 \quad (1)$$

$$Cu^+ + 3H_2O_2 \rightarrow Cu^{2+} + HO^- + {}^{\cdot}OH + 2H_2O + O_2 \quad (2)$$

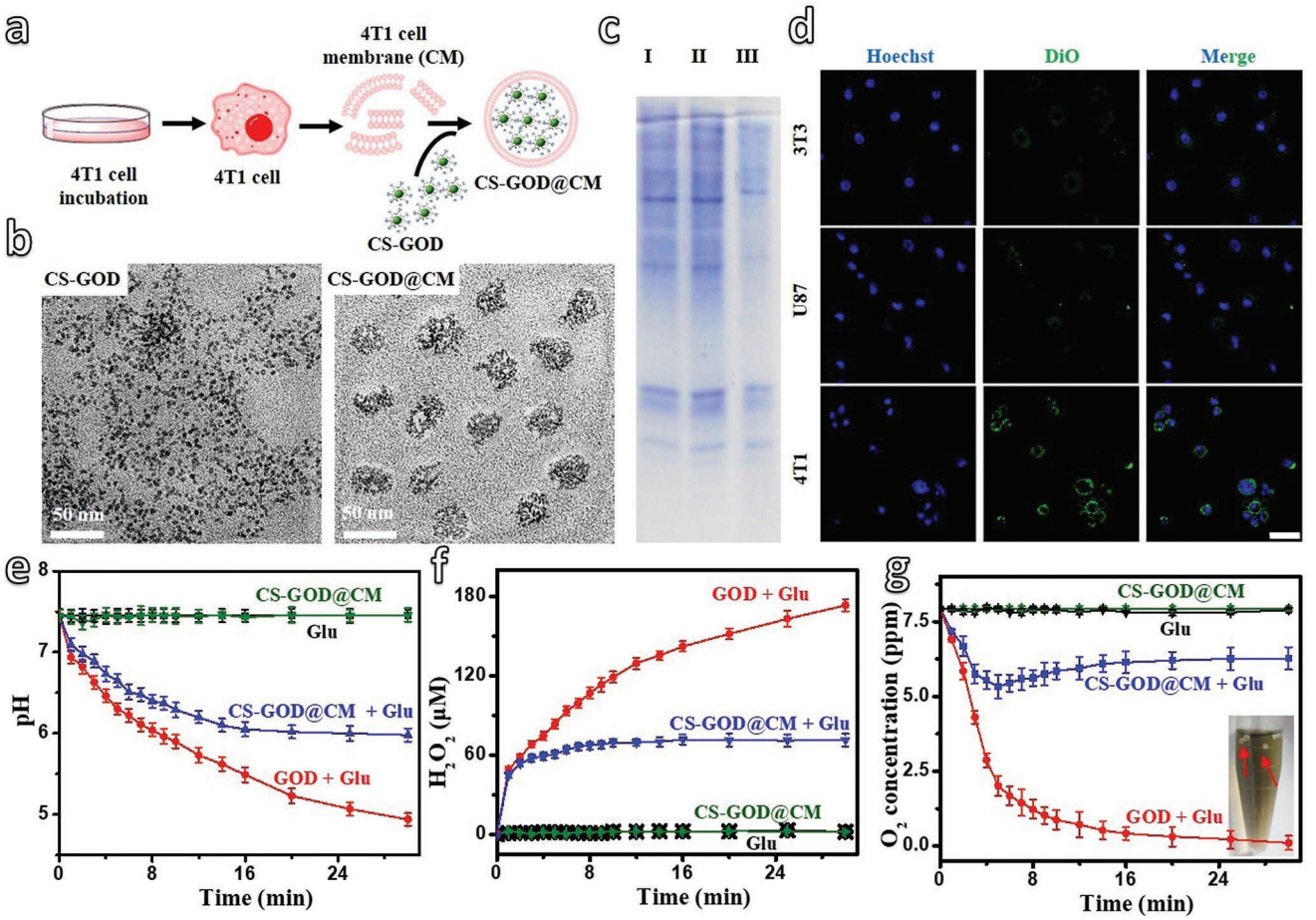

Figure 1. Preparation and characterization of CS-GOD@CM nanoparticles. a) Schematic illustration of preparation of CS-GOD@CM nanoparticles. b) Representative TEM images of CS-GOD nanoparticles and CS-GOD@CM nanoparticles. c) SDS-PAGE analysis of proteins from I) 4T1 cell lysates, II) 4T1 CM vesicles, and III) CS-GOD@CM nanoparticles. Samples were stained with Coomassie Blue for 12 h. d) CLSM images of 3T3 cells, U87 cells, and 4T1 cells, respectively, cultured with CS-GOD@CM nanoparticles for 1 h to show the homologous adhesion of nanoparticles (4T1 CMs were labeled with DiO (green FL)). The nuclei were stained blue with Hoechst 33342 (scale bar: 40 μm). e–g) The variations of time-dependent pH, H_2O_2, and O_2 of Glu solution, CS-GOD@CM nanoparticles solution, mixed solution of GOD and Glu, and mixed solution of CS-GOD@CM nanoparticles and Glu. The Glu concentration is 5×10^{-3} M. H_2O_2 concentration was detected through $Ti(SO_4)_2$ method. O_2 concentration was measured by a dissolved oxygen meter (inset: photographs of CS-GOD@CM nanoparticles mixed with Glu solution).

To compare the activity of free GOD and encapsulated GOD, the pH values of the reaction solutions were first measured, as is illustrated in Figure 1e. Obviously, in the presence of either CS-GOD@CM nanoparticles (12.5 μg mL^{-1}) or Glu (5×10^{-3} M) only, the pH values of both solutions remained constant at around 7.4, but a dramatic decrease in the pH from 7.4 to 4.9 within 30 min was observed in the solution containing free GOD and Glu, due to the oxidation of Glu into gluconic acid by GOD (Equation (1)). Compared with free GOD, the activity of GOD in the CS-GOD@CM nanoparticles was slightly decreased, as evidenced by the drop of pH from 7.4 to 5.9 within the same reaction time (i.e., 30 min). This result demonstrates that the GOD retained enough activity to catalyze the oxidation of Glu into gluconic acid and H_2O_2.

To further demonstrate the difference in their activity, the change in the H_2O_2 concentration during the oxidation of glucose was also measured by the $Ti(SO_4)_2$ method.[44] As shown in Figure 1f, more than 70×10^{-6} M H_2O_2 was generated in 30 min during the oxidation of glucose when catalyzed by CS-GOD@CM nanoparticles, which was lower than that (170×10^{-6} M) produced by free GOD under the same conditions. The difference could be due to the difference in the activity of GOD, and the fact that the CS in the CS-GOD@CM nanoparticles efficiently degraded H_2O_2 through the Fenton reaction.

The oxidation of glucose and degradation of H_2O_2 were also demonstrated by the variation in the O_2 concentration. As shown in Figure 1g, the O_2 concentration was constant in the solutions in the presence of either CS-GOD@CM nanoparticles or Glu alone, but it was decreased from 7.9 to 0 ppm during oxidation of Glu catalyzed by free GOD. Interestingly, the O_2 concentration produced by the oxidation of Glu catalyzed by CS-GOD@CM nanoparticles was first decreased from 7.9 to 5.3 ppm in the initial 5 min of the reaction, and then increased slowly to 6.3 ppm after reaction for 30 min. This result is attributed to the cascade reactions in the solution, i.e., O_2 was first consumed during the oxidation of Glu into gluconic acid and H_2O_2, the later was then degraded by CS from

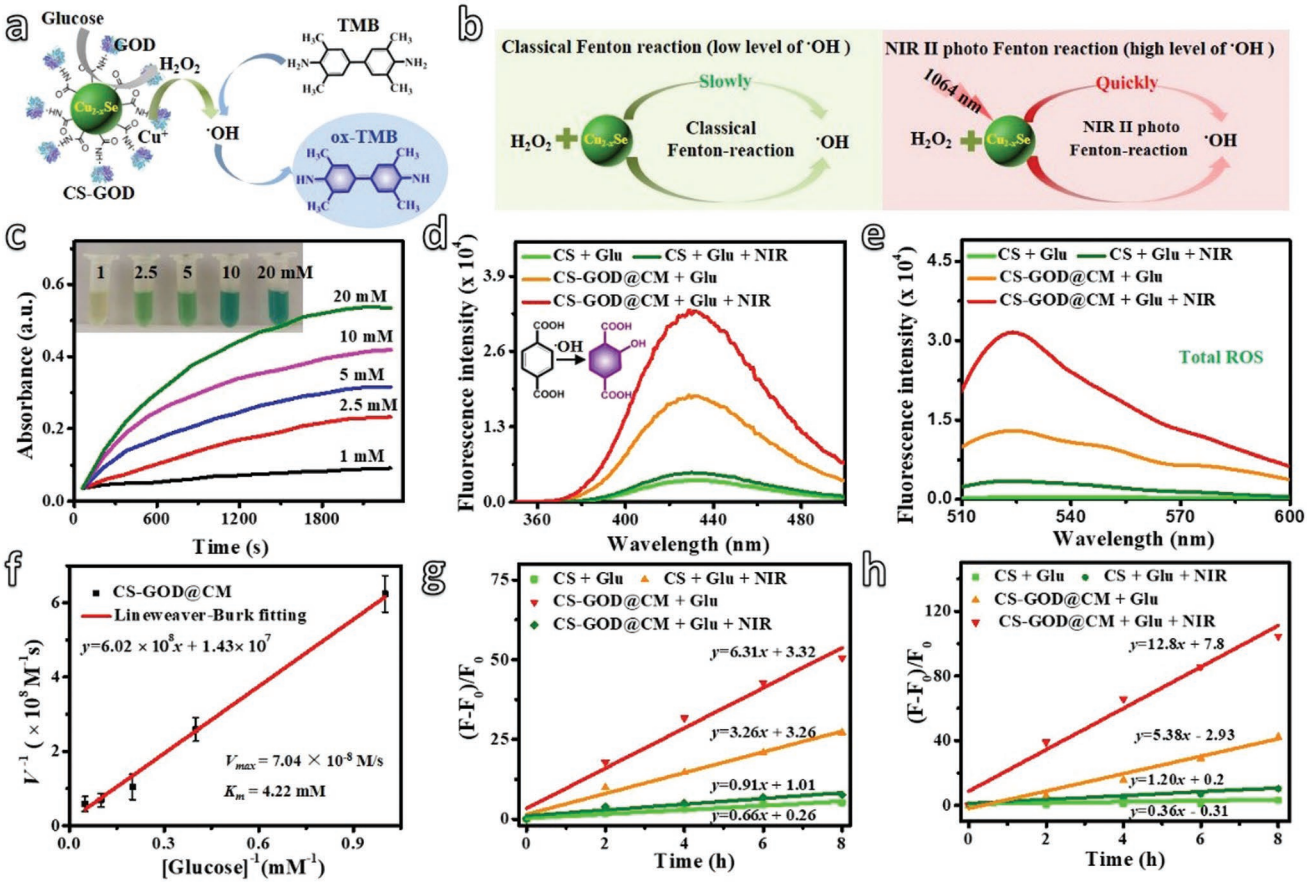

Figure 2. Characterization of cascade reactions between CS-GOD@CM nanoparticles and glucose (Glu). a) Illustration of cascade reactions for the generation of hydroxyl radicals (•OH). b) Schematic comparison of the classical Fenton reaction and the NIR-II photo-Fenton reaction. c) Time-dependence of the absorbance of oxidized 3,3′,5,5′-tetramethyl-benzidine (oxTMB) by •OH, which were generated from reactions between CS-GOD@CM nanoparticles and different concentrations of Glu (1×10^{-3}, 2.5×10^{-3}, 5×10^{-3}, 10×10^{-3}, and 20×10^{-3} M) (inset: photograph of different solutions). d) FL spectra of terephthalate (TA) oxidized by •OH radicals (as shown in inset) generated from the reactions between CS nanoparticles and Glu, and between CS-GOD@CM nanoparticles and Glu with or without 1064 nm laser irradiation. The concentrations of nanoparticles and Glu were 12.5 μg mL^{-1} and 5×10^{-3} M, respectively. The FL spectra were obtained under 488 nm excitation. e) FL spectra of DCFH-DA mixed with a solution of CS nanoparticles and Glu, and a solution of CS-GOD@CM nanoparticles and Glu with or without 1064 nm laser irradiation. The concentrations of the nanoparticles and the Glu were 12.5 μg mL^{-1} and 5×10^{-3} M, respectively. The FL spectra were obtained under 488 nm excitation. f) The dependence of the reciprocal of the reaction rate on the concentration of glucose, which was obtained by Lineweaver–Burk plotting. g) Oxidation rates of TA characterized by the variation in the FL intensity of TAOH at 428 nm. h) Oxidation rates of DCFH-DA characterized by the variation of the FL intensity of DCF at 525 nm.

the CS-GOD@CM nanoparticles to release O_2.[8] The decrease in the NIR LSPR in the UV-vis–NIR absorption spectra, as shown in Figure S2a in the Supporting Information, also supports the degradation of H_2O_2 produced from the oxidation of Glu by CS from the CS-GOD@CM nanoparticles.[45]

2.2. Catalytic Performance of CS-GOD@CM Nanoparticles Enhanced by the NIR-II Light

The above results suggest that our CS-GOD@CM nanoparticles could oxidize Glu in situ within the tumor to produce H_2O_2, and then degrade H_2O_2 to generate •OH radicals through the Fenton reaction for the treatment of cancer (Equation (2)). Therefore, 3,3′,5,5′-tetramethyl-benzidine (TMB) was applied to prove the generation of •OH radicals. The colorless TMB can be oxidized into chromogenic TMB by •OH radicals to show a unique absorption peak at 650 nm (**Figure 2**a).[46,47] Michaelis–Menten steady-state kinetics was used to assess the catalytic performance of CS-GOD@CM nanoparticles.[48] Different concentrations of Glu (i.e., 1×10^{-3}, 2.5×10^{-3}, 5×10^{-3}, 10×10^{-3}, and 20×10^{-3} M) were mixed with 12.5 μg mL^{-1} CS-GOD@CM nanoparticles for assay. The Michaelis–Menten steady-state kinetics of reactions between CS-GOD@CM nanoparticles and Glu are presented in Figure 2c,f, and Figure S2b in the Supporting Information. The time-dependent absorbance at 650 nm was plotted in Figure 2c, and a series of initial reaction rates were calculated and fitted by a Michaelis–Menten curve via the Beer–Lambert law, as shown in Figure S2b in the Supporting Information. The double reciprocal of the Michaelis–Menten equation was obtained by Equation (3) as shown in Figure 2f

$$\frac{1}{v} = \frac{K_m}{V_{max}} \cdot \frac{1}{[S]} + \frac{1}{V_{max}} \quad (3)$$

In which V_{max} is the maximal reaction velocity and K_m is the Michaelis constant. From the Lineweaver–Burk plot, V_{max} and K_m were calculated to be 7.0×10^{-8} M s^{-1} and 4.22×10^{-3} M, respectively. The results demonstrate that the reactions between CS-GOD@CM nanoparticles and Glu followed the steady-state kinetics.[49] Since the concentration of Glu in cancer cells is usually between 0.86×10^{-3} and 7.11×10^{-3} M, this ensures that enough H_2O_2 was produced by CS-GOD@CM nanoparticles through catalytic reactions to steadily and sequentially attack the tumor.[1] As shown in Figure S2c in the Supporting Information, the reaction could last for about 24 h until the Glu was consumed. The generated •OH radicals were monitored by using terephthalic acid (TA) as a probe, which can react with •OH to form 2-hydroxy-terephalic acid (TAOH) to exhibit a characteristic emission at 435 nm under excitation by 315 nm light.[28] The variation of the time-dependent FL of TAOH in Figure S2d in the Supporting Information demonstrates that the reaction time can last for 24 h.

To speed up the generation of •OH radicals, 1064 nm irradiation was applied to boost the Fenton reaction. Compared with the classical Fenton reaction, the NIR-II photo-Fenton reaction can generate •OH radicals rapidly, as schematically shown in Figure 2b. To demonstrate that NIR-II irradiation can really speed up the Fenton reaction, the generation of •OH radicals in the different cases was similarly monitored by using TA probe. It is well known that CS nanoparticles can efficiently convert NIR light into heat, and the photothermal conversion efficiency (η) of CS-GOD@CM nanoparticles was determined to be 62.9% (Figure S3a,b, Supporting Information). The temperature increment for the solution of CS-GOD@CM nanoparticles (12.5 μg mL^{-1}) under continuous irradiation by a 1064 nm laser (0.75 W cm^{-2}) for 5 min was about 10 °C (Figure S3c, Supporting Information). To minimize the influence of temperature on the reaction rate, we used pulsed irradiation to keep the temperature increase below 3 °C (Figure S3d, Supporting Information), and then investigated the effect of NIR-II irradiation on the reaction rate. The results are shown in Figure 2d,g. In the solution of CS nanoparticles and Glu, the generation of •OH radicals was very low (i.e., very weak FL of TAOH at 432 nm), whether the solution was irradiated with the 1064 nm laser or not. In the solution of CS-GOD@CM nanoparticles and Glu, large amounts of •OH radicals were produced due to the oxidation of Glu and degradation of H_2O_2, as evidenced by the strong FL of TAOH at 432 nm. After irradiation with the 1064 nm laser, the generation of •OH radicals was further improved, as demonstrated by the fact that the FL intensity of the probe was about 2.0-fold stronger than that without laser irradiation (Figure 2d). The generation rate of •OH radicals was about 1.9-fold that obtained without irradiation, illustrating that 1064 nm laser irradiation can effectively accelerate the Fenton reaction (as shown in Figure 2g), which is attributed to the efficient degradation of H_2O_2 by ultra-small CS nanoparticles under irradiation.

In addition to •OH radicals, previous report demonstrated that CS nanoparticles can also sensitize O_2 into $^1O_2$ radicals via energy transfer under the NIR irradiation.[50] To detect the total ROS, we used 2,7-dichlorofluorescin diacetate (DCFH-DA) as a probe, which can be oxidized into DCF by ROS to show FL emission at 525 nm. Figure 2e compares the FL intensity of DCF in a solution of CS nanoparticles and Glu, and in a solution of CS-GOD@CM nanoparticles and Glu, without irradiation or under irradiation by the 1064 nm laser. Similar to Figure 2d, under the NIR-II irradiation, both the solutions produced more ROS compared with the same solutions without irradiation, as evidenced by their stronger FL of DCF. In addition, the solution of CS-GOD@CM nanoparticles and Glu under NIR-II irradiation produced the maximal ROS. Their reaction rates were further quantified and are shown in Figure 2h, where the reaction rate for the Fenton reaction in the solution of CS-GOD@CM nanoparticles and Glu under the NIR-II irradiation was 2.4-fold that without laser irradiation. The faster reaction in the solution of CS-GOD@CM nanoparticles and Glu under the NIR-II irradiation further demonstrates the ability of the photo-Fenton reaction to produce more ROS.

To determine which radicals were dominant, we used the specific spin-trapping agent to distinguish different radicals, i.e., 5,5-dimethyl-1-pyrroline-*N*-oxide (DMPO) for •OH radicals and 2,2,6,6-tetramethylpiperidine (TEMP) for $^1O_2$ radicals. The electron spin resonance spectroscopy (ESR) was used to characterize their adducts DMPO-•OH and TEMP-$^1O_2$. As presented in Figure S4 in the Supporting Information, their ESR spectra clearly show characteristic quadruplets of DMPO-•OH with an intensity ratio of 1:2:2:1, and triplets of TEMP-$^1O_2$ with an intensity ratio of 1:1:1. In addition, their ESR signal was significantly increased after irradiation by 1064 nm laser light, which demonstrates the efficient degradation of H_2O_2 through photo-Fenton reaction.

Based on the above results, we measured the FL intensity of DCF before and after addition of DMPO and TEMP, which acted as scavengers of •OH radicals and $^1O_2$ radicals, respectively. The results in Figure S5 in the Supporting Information show drastic difference in the FL of DCF before and after addition of DMPO, i.e., the FL intensity was notably decreased by 72%, which indicates the dominance of •OH radicals produced from the degradation of H_2O_2 by CS-GOD@CM nanoparticles through photo-Fenton reaction. After addition of TEMP, however, the FL intensity was only decreased by 14%, which indicates the lower $^1O_2$ radicals produced and suggests more electron transfer than energy transfer occurred in CS nanoparticles under NIR-II irradiation.

2.3. Cellular Experiments with CS-GOD@CM Nanoparticles

All these results highlight the great potential of CS-GOD@CM nanoparticles for cancer therapy through the cascade reactions under irradiation by a 1064 nm laser. To investigate their performance on the cellular level, the cytotoxicity of CS and CS-GOD@CM nanoparticles toward 3T3 cells and 4T1 cells was assessed by methyl thiazolyl tetrazolium assay.[51] The results in Figure S6 in the Supporting Information show that both CS and CS-GOD@CM nanoparticles exhibited no obvious toxicity toward 3T3 cells when the nanoparticle concentration was below 12.5 μg mL^{-1} (Figure S6a, Supporting Information). In addition, the cytotoxicity of CS-GOD@CM nanoparticles was slightly higher than that of CS nanoparticles. For 4T1 cells, the cell viability was notably decreased as the concentration of CS-GOD@CM nanoparticles was increased from 1.6 to 12.5 μg mL^{-1}, in

comparison with 3T3 cells (Figure S6b, Supporting Information). The notable difference in the cytotoxicity of CS-GOD@CM nanoparticles toward 4T1 cells and 3T3 cells could be due to the sheath of 4T1 CMs on the nanoparticles, which facilitated the phagocytosis of nanoparticles by 4T1 cells. This homologous adhesion could enable nanoparticles to target 4T1 cells, and this result is consistent with that shown in Figure 1d.

To determine the optimal time when NIR-II irradiation could be applied to enhance the intracellular Fenton reaction efficiency, the concentration of H_2O_2 in cells cultured with CS-GOD@CM nanoparticles (12.5 μg mL^{-1}) was detected after different times. As shown in **Figure 3**a, the H_2O_2 concentration first increased to reach its maximum after culturing for 2 h, and then decreased with extended culture time. This result suggests that it is better to apply 1064 nm light for irradiation to achieve better Fenton reaction efficiency after 4T1 cells were cultured with CS-GOD@CM nanoparticles for 2 h. As •OH radicals were the main ROS for therapy, the cell meter mitochondrial hydroxyl radical detection kit (MHRD) was used as an •OH probe to evaluate the performance of CS-GOD@CM nanoparticles. The FL of MHRD in the CLSM images in Figure 3b clearly shows that the notable red FL observed in the cells cultured with CS-GOD@CM nanoparticles (12.5 μg mL^{-1}) was much stronger than the FL observed in cells cultured with CS nanoparticles or without nanoparticles, regardless of irradiation with or without a 1064 nm laser (0.75 W cm^{-2}). The stronger FL indicates that more •OH radicals were generated in cells after they were cultured with CS-GOD@CM nanoparticles, which is attributed to the cascade reactions in the cells, e.g., GOD from CS-GOD@CM nanoparticles catalyzed the oxidation of Glu to produce H_2O_2, which was degraded to generate •OH radicals by CS nanoparticles. Furthermore, after NIR-II irradiation for 5 min, the FL observed in the cells cultured with CS-GOD@CM nanoparticles was 2.2-fold stronger than that observed without irradiation (Figure S7a, Supporting Information). These results further support the proposition that NIR-II irradiation can enhance the catalytic performance of CS nanoparticles and enhance the Fenton reaction for degradation of H_2O_2 to form vast amounts of •OH radicals.

Furthermore, to quantify the total ROS generated in cells by CS nanoparticles and CS-GOD@CM nanoparticles with or without NIR-II irradiation, flow cytometry analysis (FCAS) and CLSM were carried out by using DCFH-DA as a ROS probe. As shown in Figure 3c, the total ROS determined by FCAS shows the similar results in Figure 3b, which further proves that CS-GOD@CM nanoparticles could effectively produce ROS and that nearly threefold more ROS were generated compared with CS-GOD@CM without irradiation group (Figure S7b, Supporting Information). The CLSM images in Figure S8 in the Supporting Information also show stronger FL in the cells cultured with CS-GOD@CM nanoparticles and then irradiated with the 1064 nm laser. These results are consistent with those shown in Figure 2d,e,g,h, and again demonstrate the enhanced Fenton reaction under NIR-II irradiation.

To determine whether the ROS generated by the NIR-II photo-Fenton reaction could kill cancer cells, cell apoptosis was quantified by FCAS, and the results are shown in Figure 3d.[52] Without laser irradiation, the apoptosis rates of 4T1 cells cultured with phosphate buffered saline (PBS), CS nanoparticles, and CS-GOD@CM nanoparticles were 8.03%, 18.85%, and 43.95%, respectively. With laser irradiation, the corresponding apoptosis rates were increased to 12.90%, 22.33%, and 80.41%, respectively, which demonstrates the significance of laser irradiation. Furthermore, live/dead staining of 4T1 cells also demonstrated that the cells could be completely killed by ROS generated by CS-GOD@CM nanoparticles under laser irradiation (Figure S9, Supporting Information), which is consistent with the results shown in Figure 3d. This means that the NIR-II photo-Fenton reaction could quickly produce abundant ROS against cancer cells compared with the classical Fenton reaction without NIR irradiation.

The depolarization of mitochondrial membranes was investigated during the ROS-mediated cell apoptosis, because it is a hallmark of apoptosis.[53] The probe 5,5′,6,6′-tetrachloro-1,1′,3,3′-tetraethyl-imidacarbocyanine iodide (JC-1) was used to characterize the depolarization of the mitochondrial membrane, because it reversibly changes its color from green to red due to the reversible formation of JC-1 aggregates upon mitochondrial membrane polarization. As shown in Figure 3e, the cells cultured with CS-GOD@CM nanoparticles exhibited weaker red FL of JC-1 aggregates and stronger green FL of JC-1 monomers, compared with those cells cultured with CS nanoparticles or without nanoparticles, illustrating the stronger depolarization of the mitochondrial membranes of the cells cultured with CS-GOD@CM nanoparticles. The depolarization of mitochondrial membranes of cells could be further enhanced by irradiation with the NIR-II light, as evidenced by the further enhancement of green FL in the cells.

These results demonstrate that increasing the intracellular H_2O_2 concentration through oxidation of Glu by GOD for the Fenton reaction catalyzed by Cu^+ ions from ultra-small CS nanoparticles is a promising way to induce apoptosis of tumor cells, which can be further enhanced by irradiation with the NIR-II light. When 1064 nm laser irradiation was applied, the apoptosis of 4T1 cells cultured with CS-GOD@CM nanoparticles was increased. After NIR-II irradiation, the ratio between apoptotic cells and healthy cells was increased by around twofold (Figure 3f).

As GOD could also oxidize Glu and cause Glu to decrease in normal tissues, the variation of Glu in the blood of mice within 12 h was monitored after tail vein injection of CS-GOD@CM nanoparticles (dose: 5 mg kg^{-1}). Figure S10 in the Supporting Information shows an obvious decrease in blood Glu from 6.9 to 4.7×10^{-3} M in the initial 2 h after administration of CS-GOD@CM nanoparticles and then spontaneous recovery to the normal level at 4.5 h post-injection. There was no pathoglycemia observed with extended observation time (Figure S10, Supporting Information), which suggests that CS-GOD@CM nanoparticles could be intravenously injected for the NIR-II photo-Fenton reaction against cancer.

2.4. Targeted Therapy of Cancer with CS-GOD@CM Nanoparticles Enhanced by the Irradiation of the NIR-II Light

The in vitro results demonstrate that the Fenton reaction catalyzed by CS-GOD@CM nanoparticles can be enhanced by increasing the H_2O_2 concentration through the oxidation of

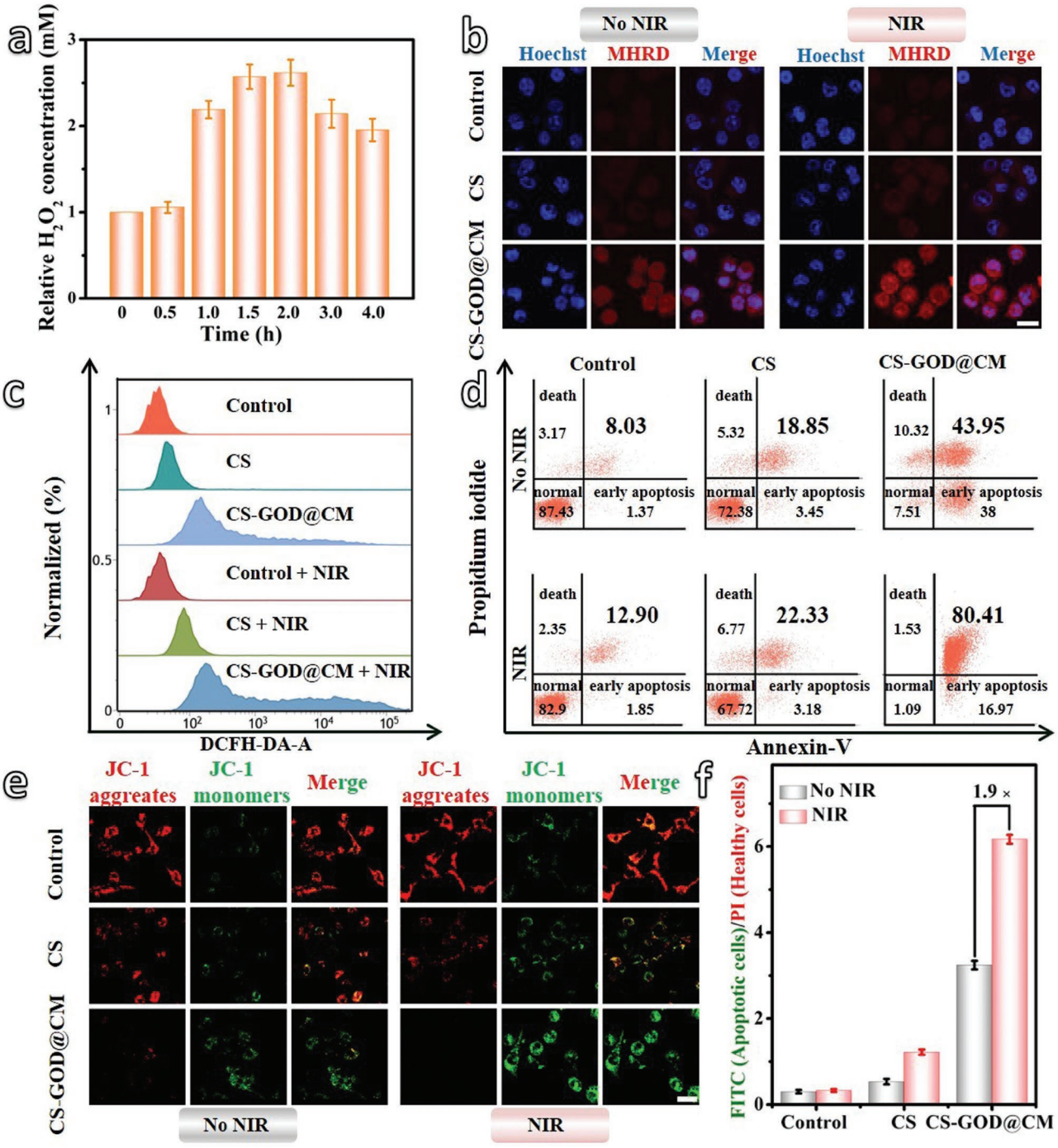

Figure 3. Characterization of the Fenton-reaction performance of CS-GOD@CM nanoparticles at the cellular level. a) Variation of the intracellular H_2O_2 concentration with time after 4T1 cells were cultured with CS-GOD@CM nanoparticles (12.5 μg mL^{-1}), as detected by the hydrogen peroxide assay kit. b–e) 4T1 cells were cultured with/without CS nanoparticles (12.5 μg mL^{-1}) or CS-GOD@CM nanoparticles (12.5 μg mL^{-1}), and then irradiated or not with a 1064 nm laser (0.75 W cm^{-2}, 5 min). b) CLSM images of cells in detection of •OH radicals by MHRD kit (scale bar 20 μm). c) FCAS of intracellular total ROS radicals by using DCFH-DA as a probe. d) Cell apoptosis ratios determined by FCAS. e) Mitochondrial depolarization of 4T1 cells indicated by the FL of aggregates and monomers of JC-1 in the CLSM images (scale bar: 20 μm). f) The ratio of apoptotic cells to normal 4T1 cells, as indicated by the ratio of the intracellular FL intensity of JC-1 aggregates (FITC) to that of JC-1 monomers (PI).

Glu and by applying NIR-II irradiation (**Figure 4**a). Since CS nanoparticles exhibit strong NIR absorbance and can efficiently convert NIR light into heat for PA imaging, PA imaging can be used to characterize the accumulation of nanoparticles at the tumor site.[54] As shown in Figure 4b,d, PA images of tumors were collected at different times after intravenous injection

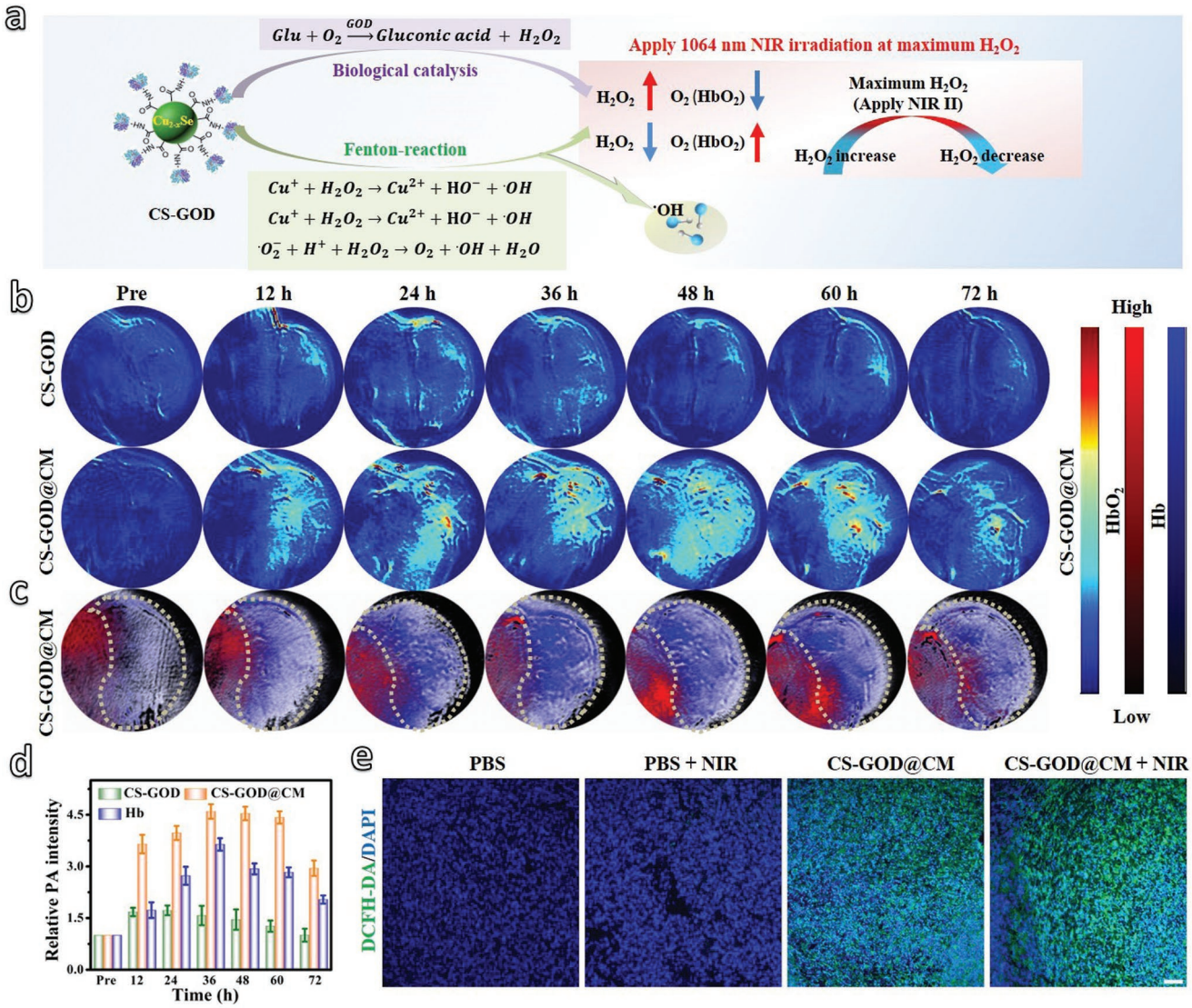

Figure 4. PA imaging guided in vivo therapy of tumors by different treatments: a) Schematic illustration of cascade reactions catalyzed by CS-GOD@CM nanoparticles and the variation of the reaction products. b) PA images of tumors from 4T1 tumor-bearing mice collected before and after tail vein injection of CS-GOD nanoparticles or CS-GOD@CM nanoparticles (dose: 5 mg kg^{-1}) at different time points. c) Time-dependent variation of oxyhemoglobin (HbO_2) and hemoglobin (Hb) concentrations in a tumor after injection of CS-CD@CM nanoparticles, separated from the PA images through image processing. d) Relative signal intensities shown in (b) and (c). e) Images of tumor tissues from different groups of mice sacrificed after 2 days of different treatments and stained with DCFH-DA (scale bar: 200 µm).

of CS-GOD nanoparticles and CS-GOD@CM nanoparticles (dose: 5 mg kg^{-1}). The PA signals at the tumor site of mice injected with CS-GOD nanoparticles reached their maximum at 24 h post-injection, which are about 1.7-fold higher than for the pre-contrast image. Then, the PA signals gradually decreased and reached their pre-contrast level at 72 h post-injection. For the mice injected with CS-GOD@CM nanoparticles (dose: 5 mg kg^{-1}), the PA signals at tumor site reached their maximum at 36 h post-injection, which were 4.6 times of the pre-contrast image and 2.7-fold higher than that obtained from mice injected with CS-GOD nanoparticles (Figure 4b,d). Furthermore, the PA signal can last longer than 72 h, which indicates the efficient accumulation and retention of nanoparticles due to the homologous adhesion effect of tumor CMs.

To determine the biodistribution of CS-GOD nanoparticles and CS-GOD@CM nanoparticles after 36 h post-injection, we used inductively coupled plasma–mass spectrometry to quantify the copper contents in major organs. The results (Figure S11a, Supporting Information) clearly demonstrate that the coating of CS-GOD nanoparticles with 4T1 CM can decrease the accumulation of nanoparticles in liver and increase their accumulation in tumor. More importantly, the copper concentration in the tumors of mice administered CS-GOD@CM nanoparticles was almost threefold that of mice injected with CS-GOD nanoparticles (Figure S11b, Supporting Information). The staining of tumor tissues clearly shows that copper stains in the tumors of mice injected with CS-GOD@CM nanoparticles were much more obvious than those of mice injected

with CS-GOD nanoparticles or not injected at all (Figure S12, Supporting Information).

The above results demonstrate that coating CS-GOD nanoparticles with 4T1 CMs can significantly improve the accumulation and retention of nanoparticles at the tumor site due to their homologous adhesion effect. To further address the homologous adhesion effect, we coated CS-GOD nanoparticles with membranes from 3T3 cells, and then did similar PA imaging with 4T1-tumor bearing mice. The results in Figure S13 in the Supporting Information show that both the accumulation of nanoparticles and their retention times were lower and shorter than those obtained with CS-GOD@CM nanoparticles. These in vivo results of homologous adhesion are well consistent with the in vitro results.

The accumulated CS-GOD@CM nanoparticles can trigger the oxidation of Glu and the degradation of H_2O_2, which leads to the time-dependent variation of oxyhemoglobin (HbO_2) or hemoglobin (Hb) in the tumor, because the oxidation of Glu consumes O_2 and the degradation of H_2O_2 produces O_2. To determine the optimal time for applying NIR-II irradiation for in vivo treatment, the time-dependent variation of Hb in the tumors of mice injected with CS-GOD@CM nanoparticles was evaluated and is displayed in Figure 4c,d. Similar to the variation of the overall PA signal, the concentration of Hb at tumor sites reached its maximum at 36 h post-injection, which means that the concentration of H_2O_2 in the tumor was the highest at this time because of the consumption of O_2 during the oxidation of Glu. The results suggest that the NIR irradiation should be performed at 36 h post-injection of CS-GOD@CM nanoparticles to enhance Fenton reaction for cancer treatment.

The power density of the 1064 nm laser and the irradiation time were set at 0.75 W cm^{-2} and 5 min to minimize the damage to normal tissues. Under continual irradiation by the 1064 nm laser for 5 min, the temperature increases in mice from both groups (i.e., the PBS group and the CS-GOD@CM group) were 6 and 11 °C, respectively (Figure S14, Supporting Information). The low temperature increases mean that 1064 nm irradiation would not cause serious damage to normal tissues and could be used to boost the Fenton reaction for cancer treatment.[55] To demonstrate such enhancement in vivo, the total ROS produced was detected using DCFH-DA stained tumor sections from different groups of mice sacrificed after 2 days treatment (Figure 4e). Obviously, much stronger green FL was present in the group of mice injected with CS-GOD@CM nanoparticles and then irradiated with the 1064 nm laser, compared with those without NIR-II irradiation, which demonstrates that the generation of total ROS in a tumor can be enhanced through 1064 nm laser irradiation.

PA imaging was also used to evaluate the vascular saturated O_2 within 4T1 solid tumors before and after 1064 nm laser irradiation (Figure S15a–c, Supporting Information). After tail vein injection of CS-GOD@CM nanoparticles (dose: 5 mg kg^{-1}), the blood oxygen saturation in the tumor was significantly decreased at 36 h post-injection, which is attributed to the consumption of O_2 by the oxidation of Glu under catalysis by GOD. This result is consistent with the variation of Hb concentration obtained from PA imaging (Figure 4c) and suggests that this was the best time for NIR-II irradiation to enhance the therapy. PA images of the tumor were recorded at 2 h post-irradiation, and the concentration of HbO_2 in the tumor was extracted from the PA images and is shown in Figure S15a in the Supporting Information. Obviously, the vascular saturated O_2 in the tumor was increased by 3.1 times in comparison with that obtained without NIR-II irradiation, because CS nanoparticles can degrade H_2O_2 into $^{\bullet}OH$ and O_2 rapidly under 1064 nm laser irradiation.

The above results demonstrate that 1064 nm laser irradiation can enhance the Fenton reaction to generate more ROS in a short time. The in vivo anticancer effect was evaluated for four groups of mice bearing the 4T1 tumors (**Figure 5**a). Two groups of mice were only injected with PBS (200 µL, PBS group) and CS-GOD@CM nanoparticle solution (dose: 5 mg kg^{-1}, CS-GOD@CM group), respectively, through their tail veins, and another two groups were also, respectively, injected with PBS and CS-GOD@CM nanoparticle solution, and then irradiated with a 1064 nm laser at 36 h post-injection. These two groups were denoted as the (PBS + NIR) group and the (CS-GOD@CM + NIR) group. Their photographs were collected and are shown in Figure S16 in the Supporting Information. Their body weights and tumor sizes were recorded every day, and the survival rates were recorded up to 50 days.

To further demonstrate the ability of CS-GOD@CM nanoparticles to kill 4T1 tumor cells, vascular endothelial growth factor (VEGF) and terminal deoxynucleotidyl transferase dUTP nick-end labeling (TUNEL) analysis, where dUTP is 4,6-diamidino-2-phenylindole, of tumors from different groups were performed, and the results are presented in Figure 5b.[56–58] Obviously, the VEGF expression in the tumors of mice injected with CS-GOD@CM nanoparticles was less than for those injected with PBS solution, whether the mice were irradiated with the 1064 nm laser or not, which means that the CS-GOD@CM nanoparticles could effectively influence the expression of VEGF in the tumor through ROS produced by the Fenton reaction. The stronger green FL from the TUNEL analysis in Figure 5b indicates that the apoptotic tumor cells were significantly increased after NIR-II irradiation, which further supports the proposition that NIR-II irradiation can effectively enhance the Fenton reaction performance to inhibit tumor growth. The absence of green FL in the tumor tissues from mice injected with PBS indicates that no apparent apoptosis occurred in the tumors, whether they were irradiated or not, which further demonstrates the enhancement of the Fenton reaction for cancer treatment by CS-GOD@CM nanoparticles under the NIR irradiation.

During 15 days of treatment, the body weights of mice in both the CS-GOD@CM and the CS-GOD@CM + NIR groups were slightly decreased in the first 3 days and then recovered to normal, in comparison with mice injected with PBS solution (Figure 5c).[59] The relative tumor volumes presented in Figure 5d demonstrates that the tumors of mice injected with PBS grew very quickly, regardless of irradiation with the 1064 nm laser. In contrast, the growth of tumors from the CS-GOD@CM group was much slower, particularly in the initial 5 days, although the tumor kept growing afterward and the photographs were measured in Figure S16 in the Supporting Information. These results demonstrate that classical Fenton reaction is not quick enough to generate large enough amounts of $^{\bullet}OH$ radicals to kill cancer cells effectively. Surprisingly, the

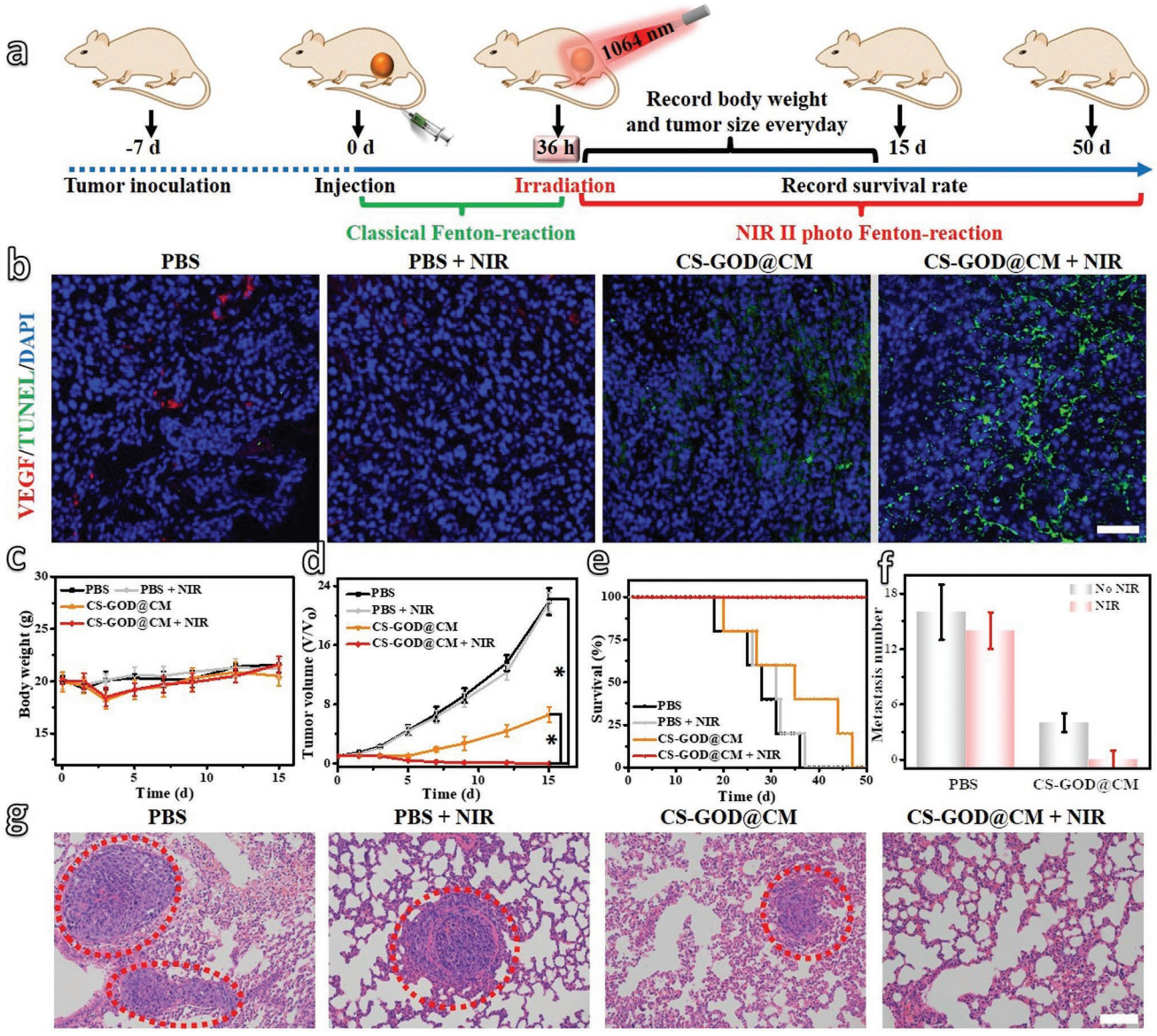

Figure 5. In vivo anticancer efficacy of CS-GOD@CM nanoparticles. a) Schematic illustration of establishment of breast cancer and therapy with CS-GOD@CM nanoparticles under 1064 nm laser irradiation at the maximum H_2O_2 concentration, guided through PA imaging. b) Representative immunofluorescence images of tumor slices from 4T1 tumor-bearing mice that received different treatments. The VEGF (red FL) was used to detect the blood vessels in the tumor, and TUNEL (green FL) was used to detect the apoptotic cells, in which the nuclei were stained with 4′,6-diamidino-2-phenylindole (DAPI, blue FL) (scale bar: 100 µm). c) Weights of mice. d) Relative tumor volumes normalized to the initial volumes ($p^* < 0.05$, $n = 3$). e) Survival rates of mice. f) Numbers of metastatic nodules in lung tissues. g) H&E staining images of metastatic nodules in lung tissues. The red circles denote the metastatic tumor (scale bar: 100 µm).

tumors in the CS-GOD@CM + NIR group gradually disappeared over 15 days, which is attributed to the enhanced Fenton reaction under NIR-II irradiation. Consequently, the mice from the CS-GOD@CM + NIR group successfully survived in good health (Figure 5e), while the mice from the other groups eventually died within 50 days.

The therapy results prove that CS-GOD@CM nanoparticles can be used for PA imaging-guided NIR-II photo-Fenton reaction treatment of solid tumors. To further demonstrate the treatment efficacy, their lung tissues were stained with hematoxylin–eosin (H&E), and the results are displayed in Figure 5g, which clearly shows that there was no metastasis in the lungs of mice from the CS-GOD@CM + NIR group 30 days post-treatment, in comparison with notable metastasis in the lungs of mice from the other groups.[60] The notable metastatic nodules in the lungs were counted and are shown in Figure 5f, the metastatic nodules in the CS-GOD@CM group were 4- and 3.5-fold lower than those in the PBS and PBS + NIR groups, respectively.[61,62] Furthermore, no metastasis was observed in the other major organs such as the heart, liver, spleen, and kidney (Figure S17, Supporting Information), which demonstrates that the breast cancer

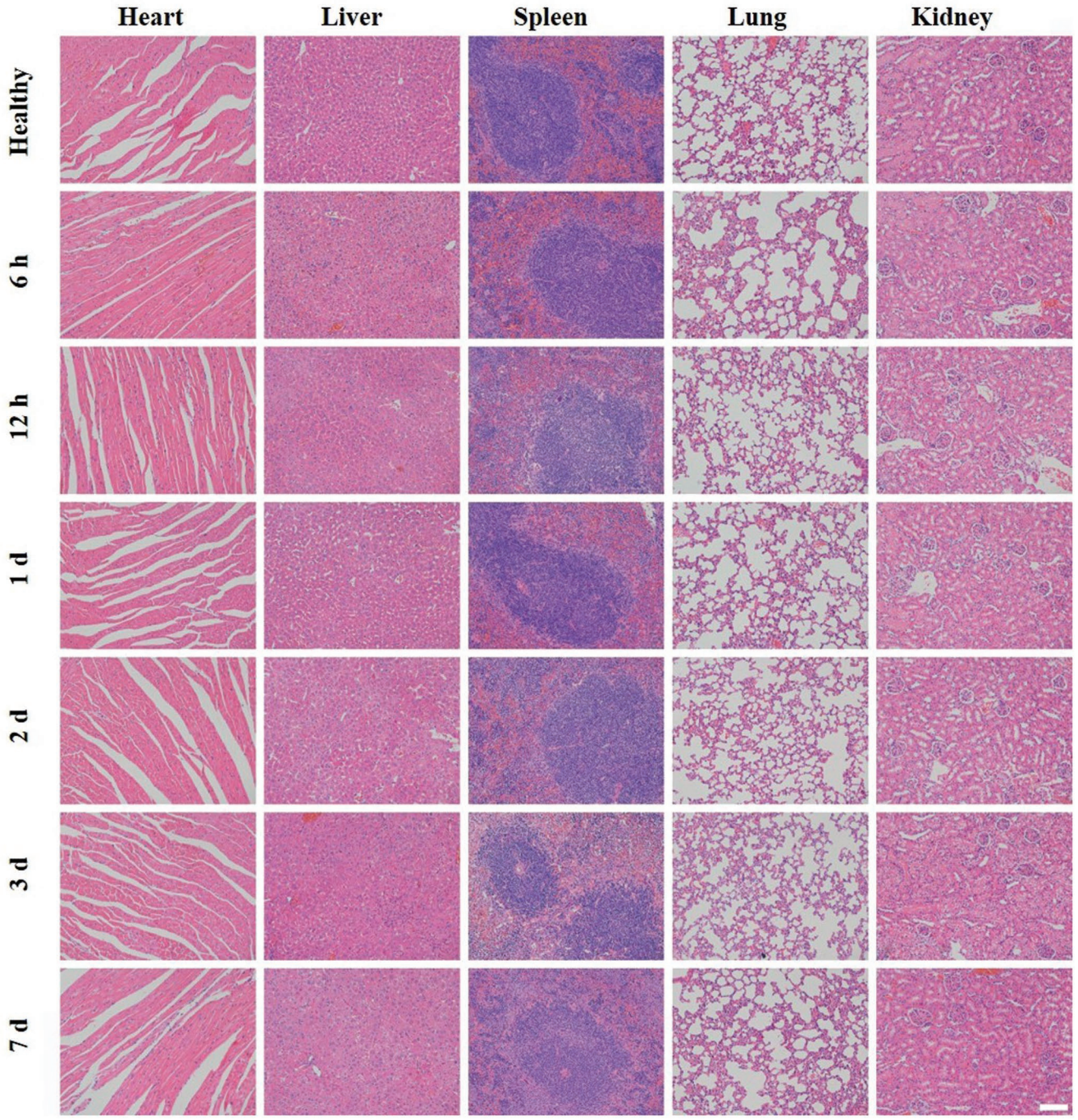

Figure 6. H&E images of major organs, including the heart, liver, spleen, lung, and kidney, collected from 4T1 tumor-bearing mice at different times after treatment with CS-GOD@CM nanoparticles in comparison with healthy mice. No obvious damage was observed. Scale bar: 100 µm.

preferred to metastasize to the lung rather than the other major organs. Additionally, the toxicity of CS-GOD@CM nanoparticles was also assessed by H&E staining of tissues of major organs (i.e., heart, liver, spleen, lung, and kidney) of mice, which were sacrificed at the different times post-injection. As shown in **Figure 6**, there was no obvious damage to the major organs in comparison with healthy mice, which demonstrates the good biocompatibility of the CS-GOD@CM nanoparticles.

3. Conclusion

In summary, we first demonstrate the H_2O_2-guided CDT of cancer enhanced by using cancer-cell-biomimetic copper selenide ($Cu_{2-x}Se$, CS) theranostic nanoparticles and the irradiation of the NIR-II light. The CS nanoparticles with strong NIR-II absorbance were conjugated with GOD for efficient in situ conversion of glucose to increase H_2O_2 for boosting the Fenton reaction, and the nanoparticles were then coated with

cancer CMs to improve their accumulation and retention at the tumor site. We demonstrate that the resultant CS-GOD@CM nanoparticles can trigger cascade reactions in vitro and in vivo, i.e., efficient oxidization of glucose and degradation of H_2O_2 through the Fenton reaction which can be drastically enhanced through irradiation by 1064 nm laser when the concentration of H_2O_2 reached the maximum, due to their strong localized surface plasmon resonance of CS nanoparticles in the NIR window. The drastic enhancement of Fenton reaction by NIR-II irradiation generated vast amounts of •OH radicals and other ROS within short time, which resulted in excellent therapeutic efficacy of breast cancer. This work highlights the great potential of the NIR-II photo-Fenton reaction in cancer treatment, and provides guidance for the rational design of high-performance biomimetic nanocatalysts for photo-Fenton reaction from the aspect of increase of reaction kinetics.

4. Experimental Section

Materials: $CuCl_2{\cdot}2H_2O$ (≥99%), Se powder (−100 mesh, ≥99.5%), sodium borohydride ($NaBH_4$, 99%), and mercaptosuccinic acid (MSA, 99%) were purchased from Sigma-Aldrich. EDC and GOD were bought from Shandong Binzhou Zhiyuan Biotechnology Co., Ltd. TA was purchased from Sinopharm Chemical Reagent Co., Ltd. DCFH-DA and the MHRD (red FL) were purchased from AAT Bioquest Inc., Thermo Fisher Scientific. Milli-Q water (>18 MΩ cm) was used in the experiments. All chemicals and reagents were used as received without any further purification.

Characterization: TEM images were captured using an FEI Tecnai G20 TEM operating at an acceleration voltage of 200 kV. DLS measurements were conducted at 25 °C on a Malvern Zetasizer Nano ZS90 equipped with a solid state He–Ne laser (λ = 633 nm). UV-vis–NIR spectra were collected on a PerkinElmer Lambda 750 UV-vis–NIR spectrophotometer. The FL spectra were recorded on an FLS980 spectrometer (Edinburgh Instruments, UK).

Synthesis of CS-GOD Nanoparticles: Se powder (0.5 mmol) was reduced by $NaBH_4$ (1.5 mmol) in 50 mL of H_2O under magnetic stirring and nitrogen protection at room temperature. Then, 5 mL of an aqueous solution of $CuCl_2{\cdot}2H_2O$ (1 mmol) and MSA (6.66 mmol) was added into the selenium precursor solution under magnetic stirring, and the reaction mixture was kept stirring for 2 h.

The resulting $Cu_{2-x}Se$ nanoparticles were centrifuged with a 30 kDa ultrafiltration tube at 4000 rpm to remove the excessive MSA, and then modified with HS-PEG-COOH at room temperature. The obtained $Cu_{2-x}Se$ nanoparticles were purified by the similar ultrafiltration to remove the free HS-PEG-COOH. The purification process was typically repeated three times using Milli-Q water as an eluent. The purified $Cu_{2-x}Se$ nanoparticles were referred to as CS NPs.

The above purified CS nanoparticle solution (400 μg mL^{-1}) was mixed with a solution of GOD (40 μg mL^{-1}) and freshly prepared EDC solution (20 μg mL^{-1}), and then rotationally shaken for 4 h at room temperature. The conjugates were similarly purified and denoted as CS-GOD nanoparticles.

Synthesis of CS-GOD@CM Nanoparticles: 4T1 CMs were prepared to coat the CS-GOD nanoparticles. 4T1 cells were first harvested and washed with PBS three times and resuspended in cold Tris buffer (pH = 7.4) (containing 10×10^{-3} M $MgCl_2$, 10×10^{-3} M Tris, and 1 × ethylenediamine tetra-acetic acid (EDTA)-free protease inhibitor) for 1 h at 4 °C, before being sonicated for 10 min in an ultrasonicator at 4 °C. The solution was then centrifuged at 600 rpm for 10 min at 4 °C, and then the supernatants were centrifuged at 11 480 rpm for 10 min, and further centrifuged at 1 10 000 rpm for 30 min. After the CMs were resuspended, the solution was extruded through 400 nm polycarbonate membranes for five cycles. Afterward, the mixture of CS-GOD nanoparticles and CMs was extruded through 200 nm polycarbonate membranes for at least five cycles. The resultant sample was denoted as CS-GOD@CM nanoparticles.

SDS-PAGE was used to characterize the proteins of membrane. The samples of 4T1 cell lysate, 4T1 CM vesicles, and CS-GOD@CM nanoparticles were mixed with lithium dodecyl sulfate loading buffer and heated at 90 °C for 10 min, and then loaded into NuPAGE Novex 4–12% bis-tris minigel of each well (20 μL of sample for each well). 3-(*N*-morpholino) propane sulfonic acid sodium dodecyl sulfate (SDS) was used as a running buffer in an electrophoresis system, stained by Coomassie Blue, and then destained overnight before imaging.

The Homologous Adhesion of CS-GOD@CM Nanoparticles: The 4T1 CM was first stained with DiO before extrusion with CS-GOD nanoparticles to make DiO-loaded CS-GOD@CM nanoparticles. 3T3 cells, U87 cells, and 4T1 cells were, respectively, seeded onto glass-bottomed dishes at a density of 8×10^4 to 1×10^5 cells per well for 24 h to allow them to attach to the surfaces of the wells. DiO-loaded CS-GOD@CM nanoparticles were cultured with the cells for 1 h. After washing three times with PBS, the cells were characterized by CLSM (λ_{ex} = 484 nm, λ_{em} = 500 nm).

Michaelis–Menten Kinetics: TMB (1.2×10^{-3} M) was used to monitor the chromogenic reaction (λ = 650 nm) between CS-GOD@CM nanoparticles (12.5 μg mL^{-1}) and glucose (Glu). The Michaelis–Menten kinetic curve of the reaction could be acquired by plotting the initial velocity against the Glu concentration. The maximal velocity (V_{max}) and the Michaelis–Menten constant (K_m) were calculated via Lineweaver–Burk plotting.

Detection of •OH Radicals and Total Radicals: TA was selected as an FL probe for specific detection of •OH radicals and DCFH-DA was applied to detect the total ROS radicals produced. CS-GOD@CM nanoparticles (12.5 μg mL^{-1}), Glu (5×10^{-3} M), and TA (6×10^{-3} M) or DCFH-DA (10×10^{-6} M) were mixed in water for 2 h, and the solution was directly irradiated by a 1064 nm laser at 0.75 W cm^{-2} for 5 min. The generation of •OH radicals was detected by measuring the FL of the mixed solution under excitation at 315 nm, and the generation of total ROS was detected by measuring the FL of the mixed solution under excitation at 488 nm.

Detection of Intracellular H_2O_2 Concentration: 4T1 cells were seeded in 6-well plates at a density of 8×10^4 to 1×10^5 cells per well and cultured in Roswell Park Memorial Institute medium (RPMI 1640) containing 10% fetal bovine serum for 24 h. Then, the cells were washed twice with PBS and incubated with CS-GOD@CM nanoparticles (12.5 μg mL^{-1}) at 37 °C under 5% CO_2 for different times, and the intracellular H_2O_2 concentration was detected by a hydrogen peroxide assay kit by using the provided protocols.

Monitoring of Intracellular •OH and Total ROS Radicals: The MHRD and DCFH-DA were used to detect •OH radicals and total ROS, respectively. 4T1 cells were seeded on glass-bottom dishes at a density of 8×10^3 to 1×10^4 cells per well for 24 h. After incubation with CS nanoparticles (12.5 μg mL^{-1}) or CS-GOD@CM nanoparticles (12.5 μg mL^{-1}) for 2 h, cells were washed twice with PBS, and then MHRD or DCFH-DA was introduced at 37 °C under 5% CO_2 for 30 min. They were then irradiated or not with a 1064 nm laser (0.75 W cm^{-2}) for 5 min, and then incubated for 2 h. Afterward, the culture medium was removed, and the cells were stained with Hoechst 33342 for 15 min for characterization by CLSM.

Testing Mitochondrial Membrane Potential: 4T1 cells were seeded on glass-bottom dishes at a density of 8×10^3 to 1×10^4 cells per well for 24 h. After incubation with CS nanoparticles (12.5 μg mL^{-1}) or CS-GOD@CM nanoparticles (12.5 μg mL^{-1}) for 2 h, they were then irradiated or not with a 1064 nm laser (0.75 W cm^{-2}) for 5 min, and then cultured for another 2 h. The cells were washed twice with PBS, stained with JC-1 (5 μg mL^{-1}) for 15 min, and then characterized by CLSM.

Tumor Model and Treatment of Tumor with CS-GOD@CM Nanoparticles: A suspension of 4T1 cells (50 μL, 5×10^6 cells) was subcutaneously injected into the flank region of the right back of 5 week old male BALB/c mice, which were used with protocols approved

by the Laboratory Animal Centre of Soochow University. After 7 days of inoculation with tumor cells, mice bearing tumors were used for treatment.

BALB/c mice bearing subcutaneous tumors 125 mm^3 in volume were divided into four groups. All groups of mice were injected with the same volume (200 µL) of solutions of PBS and CS-GOD@CM nanoparticles. The NIR irradiation was performed by using a 1064 nm laser with a power density of 0.75 W cm^{-2} for 5 min (Hi-Tech Optoelectronics Co., Ltd. Beijing, China). The body weights and tumor sizes were measured every day.

In Vivo PA Imaging of Tumor: For in vivo PA imaging, nude mice bearing subcutaneous tumors were anesthetized with 1.5% isoflurane delivered via a nose cone and injected with CS-GOD@CM nanoparticle solution (dose: 5 mg kg^{-1}) via the tail vein. The PA signals of CS nanoparticles, HbO_2, and Hb at tumor sites were separated from PA images by multispectral optoacoustic tomography (MSOT) software.

DCFH-DA and TUNEL Staining: Tumor-bearing mice were injected with solutions of PBS or CS-GOD@CM nanoparticles (dose: 5 mg kg^{-1}) via their tail veins. 36 h post-injection, the mice were intratumorally injected with DCFH-DA solution (10×10^{-6} M, 200 µL), followed by irradiation with a 1064 nm laser for 5 min (0.75 W cm^{-2}). Then, the tumors from various groups of mice were harvested and examined with CLSM to observe the FL of DCF oxidized by ROS within the tumor cells (ex/em = 488/525 nm).

To detect apoptosis of tumor cells, tumor slices were stained with TUNEL according to the One Step TUNEL Apoptosis Assay Kit. The slices were observed with a Leica microscope (DM750).

Statistical Analysis: All results of experiments were expressed as mean ± standard deviation. One-way analysis of variance statistical analysis was used to calculate the differences in data. The date were classified by the values of p and denoted by (*) for $p < 0.05$.

Supporting Information

Supporting Information is available from the Wiley Online Library or from the author.

Acknowledgements

Z.L. acknowledges support from the National Key Research and Development Program of China (2018YFA0208800), National Natural Science Foundation of China (81471657, 81527901), Jiangsu Provincial Key Research and Development Program (BE2019660), and the Program of Jiangsu Innovative and Entrepreneurial Talents. The authors also are grateful for support from the Jiangsu Provincial Key Laboratory of Radiation Medicine and Protection, the Priority Academic Development Program of Jiangsu Higher Education Institutions (PAPD). The authors thank Dr. Tania Silver for critical reading of the manuscript.

Conflict of Interest

The authors declare no conflict of interest.

Keywords

biomimetic nanoparticles, H_2O_2-guided chemodynamic therapy, NIR-II-enhanced Fenton reaction, reaction kinetics, tumor

Received: July 28, 2019
Revised: October 14, 2019
Published online: November 4, 2019

[1] W. Feng, X. G. Han, R. Y. Wang, X. Gao, P. Hu, W. W. Yue, Y. Chen, J. L. Shi, *Adv. Mater.* **2019**, *31*, 1805919.
[2] L. S. Lin, J. B. Song, L. Song, K. M. Ke, Y. J. Liu, Z. J. Zhou, Z. Y. Shen, J. Li, Z. Yang, W. Tang, G. Niu, H. H. Yang, X. Y. Chen, *Angew. Chem. Int. Ed.* **2018**, *57*, 4902.
[3] C. Zhang, W. B. Bu, D. L. Ni, S. J. Zhang, Q. Li, Z. W. Yao, J. W. Zhang, H. L. Yao, Z. Wang, J. L. Shi, *Angew. Chem. Int. Ed.* **2016**, *55*, 2101.
[4] A. D. Bokare, W. Y. Choi, *J. Hazard. Mater.* **2014**, *275*, 121.
[5] E. Ember, S. Rothbart, R. Puchta, R. Van Eldik, *New J. Chem.* **2009**, *33*, 34.
[6] A. H. Xu, X. X. Li, S. A. Ye, G. C. Yin, Q. F. Zeng, *Appl. Catal., B* **2011**, *102*, 37.
[7] S. T. Xu, X. Y. Zhu, C. Zhang, W. Huang, Y. F. Zhou, D. Y. Yan, *Nat. Commun.* **2018**, *9*, 2053.
[8] T. T. Wang, H. Zhang, Y. B. Han, H. H. Liu, F. Ren, J. F. Zeng, Q. Sun, Z. Li, M. Y. Gao, *ACS Appl. Mater. Interfaces* **2019**, *11*, 16367.
[9] L. Zhang, S. S. Wan, C. X. Li, L. Xu, H. Cheng, X. Z. Zhang, *Nano Lett.* **2018**, *18*, 7609.
[10] H. Ranji-Burachaloo, P. A. Gurr, D. E. Dunstan, G. G. Qiao, *ACS Nano* **2018**, *12*, 11819.
[11] S. Giannakis, *Appl. Catal., B* **2019**, *248*, 309.
[12] Y. Liu, W. Y. Zhen, L. H. Jin, S. T. Zhang, G. Y. Sun, T. Q. Zhang, X. Xu, S. Y. Song, Y. H. Wang, J. H. Liu, H. J. Zhang, *ACS Nano* **2018**, *12*, 4886.
[13] R. G. Zepp, B. C. Faust, J. Hoigne, *Environ. Sci. Technol.* **1992**, *26*, 313.
[14] P. Hu, T. Wu, W. P. Fan, L. Chen, Y. Y. Liu, D. L. Ni, W. B. Bu, J. L. Shi, *Biomaterials* **2017**, *141*, 86.
[15] X. J. Zhou, Y. Zhang, C. Wang, X. C. Wu, Y. Q. Yang, B. Zheng, H. X. Wu, S. W. Guo, J. Y. Zhang, *ACS Nano* **2012**, *6*, 6592.
[16] H. T. Bi, Y. L. Dai, P. P. Yang, J. T. Xu, D. Yang, S. L. Gai, F. He, B. Liu, C. N. Zhong, G. H. An, J. Lin, *Small* **2018**, *14*, 1703809.
[17] Y. He, A. del Valle, Y. Qian, Y. F. Huang, *Nanoscale* **2017**, *9*, 1559.
[18] F. B. Gao, L. J. Zhu, Y. Wang, H. J. Xie, J. F. Li, *Mater. Lett.* **2016**, *183*, 425.
[19] H. Zhang, T. T. Wang, H. H. Liu, F. Ren, W. B. Qiu, Q. Sun, F. Yan, H. R. Zheng, Z. Li, M. Y. Gao, *Nanoscale* **2019**. *11*, 7600.
[20] H. Zhang, D. Salo, D. M. Kim, S. Komarov, Y. C. Tai, M. Y. Berezin, *J. Biomed. Opt.* **2016**, *21*, 126006.
[21] G. Hong, J. T. Robinson, Y. Zhang, S. Diao, A. L. Antaris, Q. Wang, H. Dai, *Angew. Chem. Int. Ed.* **2012**, *51*, 9818.
[22] E. S. Levy, C. A. Tajon, T. S. Bischof, J. Iafrati, A. Fernandez-Bravo, D. J. Garfield, M. Chamanzar, M. M. Maharbiz, V. S. Sohal, P. J. Schuck, B. E. Cohen, E. M. Chan, *ACS Nano* **2016**, *10*, 8423.
[23] A. L. Antaris, H. Chen, K. Cheng, Y. Sun, G. Hong, C. Qu, S. Diao, Z. Deng, X. Hu, B. Zhang, X. Zhang, O. K. Yaghi, Z. R. Alamparambil, X. Hong, Z. Cheng, H. Dai, *Nat. Mater.* **2016**, *15*, 235.
[24] Y. Cai, Z. Wei, C. H. Song, C. C. Tang, W. Han, X. C. Dong, *Chem. Soc. Rev.* **2019**, *48*, 22.
[25] Y. Y. Jiang, P. K. Upputuri, C. Xie, Z. L. Zeng, A. Sharma, X. Zhen, J. C. Li, J. G. Huang, M. Pramanik, K. Y. Pu, *Adv. Mater.* **2019**, *31*, 1808166.
[26] Y. Y. Jiang, J. C. Li, X. Zhen, C. Xie, K. Y. Pu, *Adv. Mater.* **2018**, *30*, 1705980.
[27] Y. Y. Jiang, P. K. Upputuri, C. Xie, Y. Lyu, L. L. Zhang, Q. Xiong, M. Pramanik, K. Y. Pu, *Nano Lett.* **2017**, *17*, 4964.
[28] W. P. Li, C. H. Su, Y. C. Chang, Y. J. Lin, C. S. Yeh, *ACS Nano* **2016**, *10*, 2017.
[29] A. van der Vliet, H. Janssen, M. W. Yvonne, *J. Cell. Biochem.* **2014**, *115*, 427.
[30] R. A. S. Nascimento, R. E. Ozel, W. H. Mak, M. Mulato, B. Singaram, N. Pourmand, *Nano Lett.* **2016**, *16*, 1194.

[31] W. P. Fan, N. Lu, P. Huang, Y. Liu, Z. Yang, S. Wang, G. C. Yu, Y. J. Liu, J. K. Hu, Q. J. He, *Angew. Chem. Int. Ed.* **2017**, *56*, 1229.
[32] Z. Z. Yu, P. Zhou, W. Pan, N. Li, B. Tang, *Nat. Commun.* **2018**, *9*, 5044.
[33] L. H. Fu, C. Qi, Y. Ru, J. Lin, P. Huang, *Adv. Mater.* **2019**, *31*, 1808325.
[34] J. J. Li, Y. F. Li, Y. H. Wang, W. D. Ke, W. J. Chen, W. P. Wang, Z. S. Ge, *Nano Lett.* **2017**, *17*, 6983.
[35] Y. Z. Zhang, W. X. Qiu, M. Zhang, L. Zhang, X. Z. Zhang, *ACS Appl. Mater. Interfaces* **2018**, *10*, 15030.
[36] S. Y. Li, H. Cheng, B. R. Xie, W. X. Qiu, J. Y. Zeng, C. X. Li, S. S. Wan, L. Zhang, W. L. Liu, X. Z. Zhang, *ACS Nano* **2017**, *11*, 7006.
[37] Y. Liu, W. Y. Zhen, Y. H. Wang, J. H. Liu, L. H. Jin, T. Q. Zhang, S. T. Zhang, Y. Zhao, S. Y. Song, C. Y. Li, J. J. Zhu, Y. Yang, H. J. Zhang, *Angew. Chem. Int. Ed.* **2019**, *58*, 2407.
[38] S. H. Zhang, C. X. Sun, J. F. Zeng, Q. Sun, G. L. Wang, Y. Wang, Y. Wu, S. X. Dou, M. Y. Gao, Z. Li, *Adv. Mater.* **2016**, *28*, 8927.
[39] H. Zhang, T. T. Wang, W. B. Qiu, Y. B. Han, Q. Sun, J. F. Zeng, F. Yan, H. R. Zheng, Z. Li, M. Y. Gao, *Nano Lett.* **2018**, *18*, 4985.
[40] K. W. Chang, Z. H. Liu, X. F. Fang, H. B. Chen, X. J. Men, Y. Yuan, K. Sun, X. J. Zhang, Z. Yuan, C. F. Wu, *Nano Lett.* **2017**, *17*, 4323.
[41] F. X. Mao, L. Wen, C. X. Sun, S. H. Zhang, G. L. Wang, J. F. Zeng, Y. Wang, J. M. Ma, M. Y. Gao, Z. Li, *ACS Nano* **2016**, *10*, 11145.
[42] H. P. Sun, J. H. Su, Q. S. Meng, Q. S. Yin, L. L. Chen, W. W. Gu, P. C. Zhang, Z. W. Zhang, H. J. Yu, S. L. Wang, *Adv. Mater.* **2016**, *28*, 9581.
[43] J. Y. Zhu, D. W. Zheng, M. K. Zhang, W. Y. Yu, W. X. Qiu, J. J. Hu, J. Feng, X. Y. Zhang, *Nano Lett.* **2016**, *16*, 5895.
[44] J. Kim, H. Cho, H. R. Jeon, D. Kim, C. Song, N. Lee, S. H. Choi, T. Hyeon, *J. Am. Chem. Soc.* **2017**, *139*, 10992.
[45] S. H. Zhang, Q. Huang, L. J. Zhang, H. Zhang, Y. B. Han, Q. Sun, Z. X. Cheng, H. Z. Qin, S. X. Dou, Z. Li, *Nanoscale* **2018**, *10*, 3130.
[46] M. F. Huo, L. Y. Wang, Y. Chen, J. L. Shi, *Nat. Commun.* **2017**, *8*, 357.
[47] H. Ranji-Burachaloo, F. Karimi, R. Xie, Q. Fu, P. A. Gurr, D. E. Dunstan, G. G. Qiao, *ACS Appl. Mater. Interfaces* **2017**, *9*, 33599.
[48] W. B. Shi, Q. L. Wang, Y. J. Long, Z. L. Cheng, S. H. Chen, H. Z. Zheng, Y. M. Huang, *Chem. Commun.* **2011**, *47*, 6695.
[49] W. J. Luo, C. F. Zhu, S. Su, D. Li, Y. He, Q. Hang, C. H. Fan, *ACS Nano* **2010**, *4*, 7451.
[50] L. Gao, R. Liu, F. P. Gao, Y. L. Wang, X. L. Jiang, X. Y. Gao, *ACS Nano* **2014**, *8*, 7260.
[51] F. Ren, L. H. Ding, H. H. Liu, Q. Huang, H. Zhang, L. J. Zhang, J. F. Zeng, Q. Sun, Z. Li, M. Y. Gao, *Biomaterials* **2018**, *175*, 30.
[52] L. Wen, L. Chen, S. L. Zheng, J. F. Zeng, G. X. Duan, Y. Wang, G. L. Wang, Z. F. Chai, Z. Li, M. Y. Gao, *Adv. Mater.* **2016**, *28*, 5072.
[53] B. P. Shah, N. Pasquale, G. L. De, T. Tan, J. J. Ma, K. B. Lee, *ACS Nano* **2014**, *8*, 9379.
[54] C. X. Sun, Y. F. Xu, L. J. Deng, H. Zhang, Q. Sun, C. G. Zhao, Z. Li, *ACS Appl. Bio Mater.* **2018**, *1*, 673.
[55] Q. Huang, S. H. Zhang, H. Zhang, Y. B. Han, H. H. Liu, F. Ren, Q. Sun, Z. Li, M. Y. Gao, *ACS Nano* **2019**, *13*, 1342.
[56] J. Chen, H. L. Luo, Y. Liu, W. Zhang, H. X. Li, T. Luo, K. Zhang, Y. X. Zhao, J. J. Liu, *ACS Nano* **2017**, *11*, 12849.
[57] Q. Y. Jia, J. C. Ge, W. M. Liu, X. L. Zheng, S. Q. Chen, Y. M. Wen, H. Y. Zhang, P. F. Wang, *Adv. Mater.* **2018**, *30*, 1706090.
[58] J. J. Li, K. Wei, S. Zuo, Y. X. Xu, Z. S. Zha, W. D. Ke, H. B. Chen, Z. S. Ge, *Adv. Funct. Mater.* **2017**, *27*, 1702108.
[59] X. X. Jiang, S. H. Zhang, F. Ren, L. Chen, J. F. Zeng, M. Zhu, Z. X. Cheng, M. Y. Gao, Z. Li, *ACS Nano* **2017**, *11*, 5633.
[60] X. X. Jiang, Y. B. Han, H. Zhang, H. H. Liu, Q. Huang, T. T. Wang, Q. Sun, Z. Li, *ACS Appl. Mater. Interfaces* **2018**, *10*, 43396.
[61] J. C. Li, D. Cui, J. G. Huang, S. H. He, Z. B. Yang, Y. Luo, K. Y. Pu, *Angew. Chem., Int. Ed.* **2019**, *58*, 12680.
[62] J. C. Li, J. G. Huang, Y. Lyu, J. S. Huang, Y. Y. Jiang, C. Xie, K. Y. Pu, *J. Am. Chem. Soc.* **2019**, *141*, 4073.